APPLICATION OF EPRI HANDBOOK TO HSST VESSEL V-1 AND COMPARISON WITH FINITE ELEMENT ANALYSIS

P.C.M. Gortemaker*

For the evaluation of flawed ductile structures EPRI has presented an engineering approach. This consists of formulas, being collected in a reference book, which may be applied by engineers for design and analysis of flawed ductile structures.
This approach has been applied to a Heavy Section Steel Technology (HSST) test vessel for prediction of the pressure loading leading to unstable crack growth. The engineering approach has been verified by finite element method (FEM) analysis.

INTRODUCTION

In this paper attention will be given to the application of the EPRI engineering approach for prediction of the failure load of a flawed ductile vessel.

The material near the tip of a crack in a loaded medium will be highly strained, as a result of the high stresses concentrating at the crack tip. The elastic plastic behaviour of the material will have a pronounced effect on the distribution of the stresses and strains in the vicinity of the crack tip. The conditions at the crack tip can be related to the crack tip characterising parameter J.

* N.V. KEMA, Department of Mechanical and Thermohydraulic Analysis and Metallurgical Research, P.O. Box 9035, 6800 ET, Arnhem, The Netherlands.

The crack growth - either in a stable or unstable way - will be governed by this parameter J.
When the size of the plastic zone at the crack tip is sufficiently small in comparison with the geometrical structure dimensions and crack length, this can be considered as a state of Small Scale Yielding (SSY).
For these SSY conditions the parameter J can be determined from linear elastic fracture mechanics (LEFM) concepts. A limit for the application of LEFM has been given by ASTM (1).
Where this state of SSY is not fulfilled the calculation of the parameter J requires complicated elastic-plastic finite element analysis. To avoid these problems EPRI (2) has presented an engineering approach for elastic-plastic fracture analysis of flawed structures.
This approach has been applied to the HSST vessel V-1, tested by ORNL (3). This case has been used as a verification between the EPRI handbook and more expensive and time consuming advanced elastic-plastic finite element calculations. Finally these results are compared with the experimentally determined failure load.

THE EPRI ENGINEERING APPROACH

Estimation procedures for the crack tip characterising parameter J have been developed for a variety of flawed structural geometries for el.-pl. conditions throughout the range of deformation of SSY to Fully Plastic Yielding (FPY). These procedures involve a simple summation of the tabulated FPY solutions and existing elastic solutions.
The prediction of crack growth is based on so-called crack driving force solutions related to the experimentally determined material J resistance curve. The procedure will characterize the crack growth behaviour and will predict the crack growth process from crack initiation via stable growth to instability.
In this paragraph attention will be given to the following consecutive stages in application of the EPRI approach for the prediction of the failure load of the HSST vessel V-1.

- Calculation of the parameter J.
- Prediction of failure load using the engineering approach.

Calculation of the parameter J

The elastic-plastic formulas given in reference (2) are based on the stress-strain curve following the Ramberg Osgood stress-strain law. These curves are described by:

$$\frac{\varepsilon}{\varepsilon_o} = \frac{\sigma}{\sigma_o} + \alpha \left(\frac{\sigma}{\sigma_o} \right)^n \qquad (1)$$

where σ_o is yield stress, ε_o is yield strain.
For the symbols used in this paper reference is made to the list of symbols at the end of this paper.

By an appropriate choice of the parameter α and the strain hardening index n one should fit this relation to the experimental stress-strain curve. However in the experimental tensile stress-strain curve for A508 class 2 steel of the V-1 vessel an initial plastic plateau is present, which cannot be modelled by eq. (1). This makes a unique choice of the power law parameters impossible. To verify the sensitivity of the choice of these parameters on the EPRI solution, the stress strain curve has been modelled for two sets of parameters, as shown in figure 1. The parameters α, n, σ_o, and ε_o are listed in TABLE 1.

The elastic-plastic solution for J is obtained by superimposing the elastic and fully plastic contribution according to the following equation:

$$J = J^e (a_e) + J^p (a,n) \qquad (2)$$

where a_e represents Irwin's effective crack length, modified to account for strain hardening.

$$a_e = a + \phi\, r_y \qquad (3)$$

where

$$r_y = \frac{1}{\beta\pi} \left(\frac{n-1}{n+1} \right) \left(\frac{K_I}{\sigma_o} \right)^2 \qquad (4)$$

and

$$\phi = \frac{1}{1 + (P/P_o)^2} \qquad (5)$$

where for an axially cracked pressure vessel $\beta = 6$.

P_o is the limit pressure in the perfectly plastic case. A lower bound value, for a vessel with an inside axial crack, is determined from the biaxial stress state determined by the combined plane strain, plane stress condition across the ligament and is given by:

$$P_o = \frac{2}{\sqrt{3}} \cdot \frac{c.\ \sigma_o}{R_c} \qquad (6)$$

where $R_c = R_I + a$

The geometrical vessel properties are given in TABLE 2. The solutions in the EPRI handbook are only applicable to inside cracked vessels. However the HSST V-1 vessel is outside cracked. In combination with the solutions given in the supplement to the EPRI handbook, reference (4), the EPRI approach is also applied for the outside cracked pressure vessel V-1.

For the outside cracked vessel the lower bound value of the limit pressure is given by:

$$P_o = \frac{2}{\sqrt{3}} \cdot \frac{c.\ \sigma_o}{R_I} \qquad (7)$$

The elastic contribution $J^e\ (a_e)$

In linear elastic fracture mechanics the parameter J can be determined from the stress intensity factor K_I.

For plane strain conditions this relation can be written by:

$$J^e = K_I^2 / E' \qquad (8)$$

Where $E' = E/(1 - \nu^2)$

This relation will also be applied for an axially cracked pressure vessel. The stress intensity factor for an inside cracked vessel can be determined from the solutions given by:

$$K_I = \frac{2P\ R_o^2}{R_o^2 - R_I^2} \cdot \sqrt{\pi a}.\ \ F_1\ (a/b,\ R_I/R_o) \qquad (9)$$

where F_1 has been derived from figure 160, given by Rooke et.al. (5).

For outside cracked vessels the stress intensity factor can be given by:

$$K_I = \frac{2\,P\,R_I^2}{R_o^2 - R_I^2} \cdot \sqrt{\pi a}\;\; F_o\,(a/b,\; R_I/R_o) \qquad (10)$$

where F_o has been determined from figure 156, given in reference (5).

For the dimensions and properties of the HSST V-1 vessel, given in TABLE 2, the values of F_1 and F_o are given in figure 2.

The full expression for the elastic contribution to J can be written as:

$$J^e = f_1\,(a_e;\; R_I/R_o).\; P^2/E' \qquad (11)$$

where for an inside cracked cylinder

$$f_1 = 4\,\pi a \left(\frac{R_o^2}{R_o^2 - R_I^2}\right)^2 F_1^2\,(a/b;\; R_I/R_o) \qquad (12)$$

and for an outside cracked cylinder

$$f_1 = 4\,\pi a \left(\frac{R_I^2}{R_o^2 - R_I^2}\right)^2 F_o^2\,(a/b;\; R_I/R_o) \qquad (13)$$

Fully plastic contribution J^p

The fully plastic solutions for J can be determined from the formulas and tables given in reference (1). The expression can be written as:

$$J^P = \alpha\;\sigma_o\;\varepsilon_o\;c\;\frac{a}{b}\;h_1\,(a/b,\; n;\; R_I/R_o)\;(P/P_o)^{n+1} \qquad (14)$$

For an axial inside cracked cylinder the dimensionless function h_1 is given as functions of a/b and n for different values of R_I/R_o.

From these functions, h_1 has been determined as a function of a/b for n=5 and n=11, as shown in figure 3.
For the outside cracked vessel h_1 has been determined from the EPRI supplement (4), where h_1 has been given as a function of R_I/b for a hardening index n=5 and a/b= 0.5. From these limited data only a single value for h_1 can be derived. For the V-1 vessel h_1 = 8.

Prediction of failure using the engineering approach

By using the EPRI handbook one have to model the semi elliptical surface crack as an infinite longitudinal semi elliptical surface crack. Because of this approximation no conclusions can be drawn with respect to the conservatism of the engineering approach. The crack driving force diagrams are calculated with the el.-pl. J solutions. The full expression for J can be given by:

$$J + f_1 (a_e; R_I/R_o) \frac{P^2}{E'} + \alpha \sigma_o \varepsilon_o c \frac{a}{b} h_1 (a/b,n; R_I/R_o)(P/P_o)^{n+1} \quad (15)$$

Using the results given in figures 2 and 3 the J-a curves can be calculated for several pressures. This has been done for inside as well as for outside cracked cylinders, as shown in figures 4 and 5.
The crack growth behaviour is predicted from the comparison between the J-a curves and the material resistance to crack growth (the J_r curve) determined experimentally.
For prediction of failure specific attention will be given to the transition from stable to unstable crack growth.
Failure is predicted at the load where the J-controlled crack growth becomes unstable. The crack growth will be unstable at the point of tangency of the constant load curve and the J_r curve. For application of this procedure one needs a material resistance curve for the material to be considered.
For the material of the V-1 vessel such a curve is given, for several temperatures, in reference (6). However this curve is only applicable for stable crack growth up to 0.05 inch (0.00127 m).
This is only the very beginning of the resistance curve.

Due to the lack of any other information of R-curves for the steel of the V-1 vessel, the curve for A533B steel, given in the EPRI handbook, has been used for the calculations.

Application of this curve will lead to a prediction of stable crack growth over about a quarter of a inch.

The calculated failure loads are given in TABLE 3 at the end of this paper. From these results one can conclude that in this case the choice of the power law parameters affect the predicted failure loads by about 12 %. The power hardening corresponding to n=5 predicts a lower failure load, which may be caused by the larger deformations at the lower stress levels in comparison to the n=11 power hardening index.
The predicted failure load is considerable smaller than the experimental determined pressure load. This is a result of the rough modellisation of the semi elliptical surface crack.

FEM ANALYSIS

For these analysis the 81 version of the general purpose finite element program ADINA (7) has been used.
As no special fracture mechanics options are available, in this version the crack tip characterising parameter J has been determined from the rate of decrease of potential energy per unit thickness with respect to the crack size.

$$J = - \frac{dU}{da} \qquad (16)$$

For the construction of the constant load J-a curves, one can suffice with calculations of J at constant loads for different crack lengths.
The decrease of potential energy can be expressed by:

$$dU = -{}_o\int^P {}_o\int^{2\pi} u(a+da)\, R_I\, d\theta\, dP + {}_o\int^P {}_o\int^{2\pi} u(a)\, R_I d\theta\, dP +$$

$$- 2\,{}_o\int^P {}_{R_I}\int^{R_I+a} v\,(a+da)\, dr\, dP + 2\,{}_o\int^P {}_{R_I}\int^{R_I+a} v\,(a)\, dr\, dP \qquad (17)$$

Last two terms are only applicable for inside cracks.

u is the radial displacement and v is half the crack opening displacement, considered across the crack-surface of an inside crack.

prediction of failure loads by FEM analysis

Due to the axial loading at the pressure vessel ends, the axial straining will be nonzero. However in many FEM analyses this condition will be approximated by the more simple 2-D plane strain conditions. To verify this simplification, comparative analyses are carried out for 2-D plane strain conditions and 3-D conditions, where the shear deformations γ_{rz} and $\gamma_{\theta z}$ are set to zero.
Because of the axi-symmetry, with respect to the plane of the crack, only one half of the cylinder has been considered. The finite element modelling is shown in figure (6). For the 2-D plane strain analysis the finite element modelling of the cylindrical cross section in the r-Θ plane is identical to the 3-D modelling. To account for the singular strains at the crack tip the midside nodes of the elements at the crack tip have been moved to a quarter of the element side.
Both 2-D and 3-D analyses have been applied for the outside cracked V-1 vessel. The data are given in TABLE 2. The stress-strain curve has been fitted to the experimental curve, which is shown in figure 1. The upper yield stress has been neglected and has been replaced by the lower yield stress.
J has been calculated from eqs (16) and (17).
This has been done for 3 different crack lengths.
From these results the crack driving force diagrams (CDF) have been determined, as shown in figure 7. Unstable crack growth is predicted at a load of 145 MPa.
The difference between the results of the 2-D and 3-D analyses lies within 1 %. Because of this good agreement the CDF diagrams for the inside cracked vessel are determined from 2-D analysis.The calculated CDF diagrams are given in figure 8. Unstable crack growth of the inside crack is predicted at a load of 131 MPa. For comparison with the loads determined from the EPRI handbook, these results are given in TABLE 3. The experimental failure load, also given, is considerably higher.

This is due to the very simplified modelling of the semi elliptical surface crack as an infinite long axial surface crack.
The failure loads, calculated from the FEM analyses, are higher than those determined from the engineering approach. This may be partially due to the rather coarse finite element discretisation, but also to the modelling of the stress-strain curve. At the stresses below yield stress, the power law approximation leads to a higher straining in comparison to the experimental stress-strain curve, being used in FEM analysis.
This results in a large plastic contribution to JP of the engineering approach, which will lead to prediction of lower loads.
Finally it is noted that the failure loads for the outside crack are higher than those for inside cracks.

CONCLUSION

The results obtained from the engineering approach are affected by the choice of the parameters used for modelling the stress-strain curves. This is found from analyses with two different power law approximations for the material of the axially cracked HSST vessel V-1. In comparison to upper bound approximations, the lower bound approximations tend to conservative results. This result is also confirmed by FEM calculations, where for stresses below yield stress the straining is smaller in comparison to the straining of the power law approximations.
This is also one of the reasons for the higher failure loads predicted by the FEM calculations.
The J values determined from the 2-D plane strain and 3-D constant strain finite element modellisations of the axial cracked pressure vessel are in excellent agreement.
The lack of adequate information about material properties needed for the calculation of stable crack growth, leads to difficulties in the application of the procedures given in the EPRI handbook. Especially problems arise with respect to the data needed for the material resistance (J_r-a) curves, which also may be affected by temperature.
The calculated failure loads are well below the experimental failure load.

However due to the simple modellisation of a semi elliptical surface crack by an infinite longitudinal semi elliptical surface crack no conclusions with respect to the conservatism of the EPRI engineering approach can be made.

TABLE 1 - Power law parameters

Parameter	curve I	curve II
α	7.0	3.0
n	5	11
σ_o	483 MPa	496 MPa
ε_o	0.00233	0.00240

TABLE 2 - Data for fracture analysis of HSST test vessel V-1

Material	A508, Class 2 forging steel
Test temperature, °C	54
Flaw dimensions, m	
Depth (a)	0.065
Surface length (2l)	0.2095
Vessel dimensions, m	
Inside radius	0.3429
Outside radius	0.4953
Wall thickness	0.1524
Young's modulus, MPa	$206.8 * 10^3$
poisson's ratio	0.3

TABLE 3 - Failure loads

Calculation method or experiment	Crack location	Pressure at Failure (MPa)
EPRI (n=5)	Outside	117
FEM	"	145
Experiment	"	199
EPRI (n=5)	Inside	110
EPRI (n=11)	"	124
FEM	"	129

SYMBOLS USED

a, a_e	= crack length, effective crack length
b	= wall thickness
c	= size of ligament
E	= Young's modulus
J	= crack tip characterising parameter
J^e, J^p	= elastic, plastic contribution to J
K_I	= stress intensity factor for mode I
n	= power law hardening index
P	= internal pressure
P_o	= limit pressure in perfectly plastic case
R_I, R_o	= inside, outside radius of cylinder
r	= radial coördinate
r_y	= plastic zone size
U	= potential energy
u	= radial displacement
v	= tangential displacement
α	= power law parameter
β	= factor for calculation of plastic zone size
γ_{rz}, $\gamma_{\theta z}$	= shear deformation in r-z and θ-z planes
ε, ε_o	= strain, yield strain
θ	= tangential coördinate
ν	= poisson's ratio
σ, σ_o	= stress, yield stress
Φ	= factor for calculation of effective crack length

REFERENCES

(1) ASTM 1970 Annual Book of ASTM Standards. Pt. 31, P.911. American Society for Testing Materials, Philadelphia.

(2) Kumar, V., German, M.D., and Shih, C.F., "An Engineering Approach for Elastic-Plastic Fracture Analysis", EPRI NP-1931, Topical Report, Research Project 1237-1, General Electric Company, Schenectady, NY, USA, July 1981.

(3) Derby, R.W., Merkle, J.G., Robinson, G.C., Whitman, G.D., and Witt, F.J., "Test of 6-Inch-Thick Pressure Vessels. Series 1: Intermediate Test Vessels V-1 and V-2", ORNL-4895, Oak Ridge National Laboratory, Oak Ridge, Tenn., USA, Febr. 1974.

(4) Kumar, V., German, M.D., Wilkening, W.W., Andrews, W.R., de Lorenzi, H.G. and Mowbray, D.F., "Advances in Elastic-Plastic Fracture Analysis". NP 3607, Research Project 1237-1, General Electric Company, Schenectady, N.Y., USA, August 1984.

(5) Rooke, D.P. and Cartwright, D.J., "Compendium of stress Intensity Factors", Her Majesty's Stationary Office, Londen, G.B., 1976.

(6) Zahoor, A. and Paris, P.C., "A Preliminary Fracture Analysis on The Integrity of HSST Intermediate Test Vessels". Nureg/CP-0010, CSNI Report No. 39, Proc. of the U.S. Nuclear Regulatory Commission, CSNI Specialist Meeting on Plastic Tearing Instability, St. Louis, USA, Sept. 25-27, 1979.

(7) ADINA Users Manual, Report AE 81-1, ADINA TM. Adina engineering AB, Västeras, Sweden, Sept. 1981.

Acknowledgement The author is indebted to H. Spiele for his assistance in preparation of the FEM calculations.

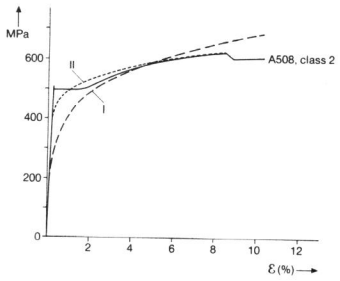

Figure 1 Stress- strain curves for A508-Class 2 steel.

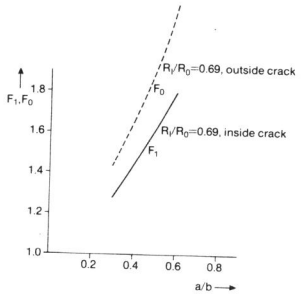

Figure 2 F_1 and F_o as a function of a/b for R_I / R_o = 0.69.

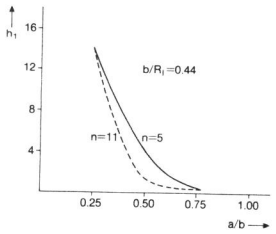

Figure 3 h_1 as a function of a/b.

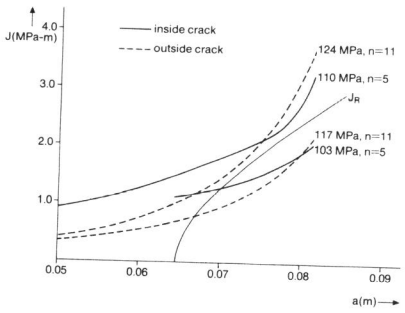

Figure 4 EPRI C.D.F. diagram for inside cracked cylinder.

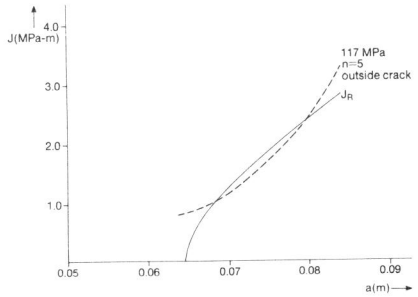

Figure 5 EPRI C.D.F. diagram for an outside cracked cylinder.

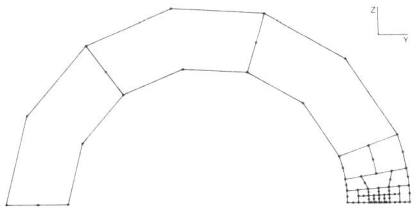

Figure 6 Finite element mesh.

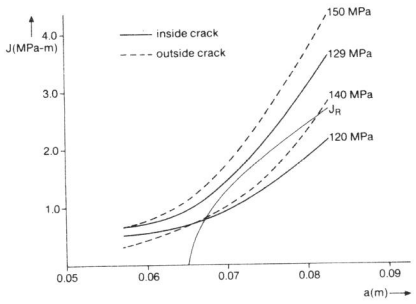

Figure 7 Crack driving force diagrams determined from the ADINA FEM calculations.